lubricants

MDPI

Article

Dry-Sliding Behavior and Surface Evolution of SLS-Manufactured Glass Bead-Filled Polyamide 12 Bearings

Ivan Simonović *, Dragan Milković, Žarko Mišković and Aleksandar Marinković

Faculty of Mechanical Engineering, University of Belgrade, 11000 Belgrade, Serbia; dmilkovic@mas.bg.ac.rs (D.M.); zmiskovic@mas.bg.ac.rs (Ž.M.); amarinkovic@mas.bg.ac.rs (A.M.)
* Correspondence: isimonovic@mas.bg.ac.rs

Abstract

This study investigates the tribological behavior of selective laser-sintered (SLS) sliding bearings under dry-sliding operating conditions. These polyamide-12 bearings reinforced with glass beads (PA 3200 GF) were tested against a stainless-steel sleeve in three different pressure–velocity (PV) regimes that represent real operating conditions. The coefficient of friction (COF) and contact temperatures were monitored throughout the experiment, while the specific wear rate was quantified based on mass loss measurements. The evolution of surface topography was analyzed using roughness parameters of the Abbott-Firestone family. Scanning electron microscopy (SEM) analysis was performed to identify the dominant wear mechanism. The results show a pronounced running-in phase, after which a stable thermomechanical equilibrium occurs in all regimes. Heavy-loaded regimes increase temperature but accelerate surface adaptation and lower stable coefficients of friction. Lower load regimes have the lowest thermal load but higher friction due to lower real contact. The medium PV regime has a low COF and moderate temperature rise, while peak and core roughness metrics increase more significantly. These results provide an experimentally based insight into the influence of the load regime on the tribological behavior and topography of the SLS-made polymer sliding bearings, thus contributing to a deeper understanding of their operation in real dry-sliding conditions.

Keywords: sliding bearings; selective laser sintering; PA 3200 GF; tribological performance; dry-sliding conditions

1. Introduction

Sliding bearings are machine elements that enable the transmission of power and torque; they serve to carry loads with minimal friction. Tribological mechanisms have a significant influence on the efficiency and service life of machines, primarily through the coefficient of friction (COF), surface morphology change, wear and contact temperature [1]. Conventional, usually metal, sliding bearings rely on an external lubricant supply and operate in a hydrodynamic lubrication system. These systems require additional equipment for the lubricant supply, so their maintenance as well as the management of their use, most commonly mineral oils, increases operating costs and represents a potential environmental hazard. In the context of sustainable mechanical engineering, there is a need for the development of sliding bearings that operate in lubrication-free conditions, with appropriate load-carrying capacity and service life [1,2].

Polymer-based bearings and their composites show significant potential for successful operation as a self-lubricating and maintenance-free solution. Compared to metals,

Check for updates

Received: 30 November 2025
Revised: 5 January 2026
Accepted: 6 January 2026
Published: 9 January 2026

Copyright: © 2026 by the authors. Licensee MDPI, Basel, Switzerland. This article is an open access article distributed under the terms and conditions of the Creative Commons Attribution (CC BY) license.

polymers are characterized by low mass and corrosion resistance and can operate in lubrication-free conditions, thus eliminating lubricant supply subsystems and reducing the risk of environmental contamination with mineral oils [3,4]. By using polymers with solid lubricants and composites reinforced with graphite, graphene, molybdenum disulfide, polytetrafluoroethylene (PTFE), glass fibers, glass beads, or ceramic particles, it is possible to significantly reduce the coefficient of friction and specific wear while maintaining the necessary elasticity and load-carrying capacity [3,5–8]. Research shows that carefully engineered polymer composites can match and even exceed the friction and wear performance of metal bearings, especially in aggressive environments, oscillatory regimes, and conditions with limited lubrication, corrosion risk, and critical requirements [3,4,8].

The development of additive manufacturing (AM), a paradigm based on the addition of material, opened up a space for utilizing new materials and improving the design of sliding bearings. Among the AM processes, selective laser sintering (SLS) stood out as particularly favorable for the production of functional, end-use, load-carrying machine parts since it enables the creation of complex geometries directly from polymer powder [9]. A key advantage of the SLS process is that it does not require support structures; enables efficient use of powder; and offers the possibility of adjusting production parameters such as laser power, hatching space, powder bed temperature, and build orientation to obtain high-quality parts [9–11]. These parameters influence the porosity, microstructure, and mechanical properties of the manufactured part [10–13]. For tribological applications, SLS enables the use of high-performance materials, including polyamide 12 (PA12) and its composites reinforced with glass beads, glass fibers, carbon fibers, and solid lubricants, which can be optimized to improve tribological characteristics under lubrication-free conditions [6,10,14–17].

Polyamide 12 is one of the most commonly used thermoplastics due to its favorable processability, dimensional stability, and balanced mechanical properties. By adding glass beads to the PA12 matrix, a glass bead-filled composite, also known as PA 3200 GF, is obtained. This material was developed for making stiff, dimensionally stable parts under load, such as sliding bearings. Experimental tests show that reinforcement with glass beads increases the modulus of elasticity and stiffness of pure PA12, while the mechanical response still exhibits a certain sensitivity to powder bed temperature and build orientation [11,13,18,19]. The interaction between the glass reinforcement and the polymer matrix can lead to a decrease in fracture toughness, tensile strength, and fatigue life, as well as to decreased ductility compared to neat PA12 or short-fiber-reinforced grades [12,18–20]. These tests indicate that both the material formula and the production parameters must be carefully optimized in order to achieve a balance between stiffness, strength, and damage tolerance for demanding operating conditions [12,13,19,20].

Tribological tests of SLS-produced PA12 and their composites are usually conducted using standardized methods such as pin-on-disc or block-on-disc. For short glass fiber-reinforced PA12 in conditions of sliding on steel, it was shown that the amount of fibers and the applied load have a key effect on friction and wear, while the fiber orientation itself had a relatively small effect [5]. Orientation-dependent tests on SLS-manufactured PA 3200 GF showed marked anisotropy in wear: specimens with layers perpendicular to the sliding plane showed more adhesive wear but significantly lower COF and material loss [14]. Other studies have shown that the addition of solid lubricants such as MoS_2, PTFE, and graphite can significantly reduce friction and specific wear, in some cases by more than 50%, as well as change the dominant wear mechanism [6,15]. PA12 composites made by SLS, reinforced with carbon fiber and graphite, show reduced friction, increased resistance to wear, and, in certain cases, almost complete tribological independence from the orientation of production [7,16,17]. The literature indicates that SLS-produced PA 12 composites,

including PA 3200 GF, are a reliable choice for applications in dry-sliding conditions, provided careful selection of composition and manufacturing parameters [6–8,10,14–16].

In contrast to extensive tests of tribological samples, a relatively small number of studies dealt with additively manufactured sliding bearings with real geometries and real operating conditions. Research on textured journal bearings made by fused deposition modeling (FDM) with acrylonitrile butadiene styrene (ABS), polylactic acid (PLA), and nylon showed that nylon-based bearings show the best combination of low friction and low wear rate among the tested materials [21]. The authors in [22] compared SLS and FDM methods for manufacturing bearings based on aluminum and nylon and showed that SLS nylon bearings have low friction in a certain range of loads and speeds. By examining MultiJet-printed bearing sleeves, the authors showed in [23] that internal fit and applied load have the greatest impact on performance at low speeds. In the previous work [24] in which we examined SLS-made PA12 bearings, it was shown that for the corresponding pressure–velocity (PV) regimes, we have a low and stable coefficient of friction, while the contact temperature remains in the safe zone, thus confirming the feasibility of additively manufactured bearings in real operating conditions.

Despite the progress mentioned, there is still a significant gap in research. Most tribological studies of SLS-fabricated PA12 and PA 3200 GF are based on simple sample geometries, short-term tests, or a single test regime, which makes it difficult to directly apply the results to real sliding bearings. For PA 3200 GF, experimental data on the influence of the PV regime on the running-in process, stabilization of the tribological response, and accompanying changes in topographic parameters relevant to load-carrying capacity remain very limited. A clearer understanding of these relationships is key to defining PV limits, avoiding deformation due to overheating, and achieving stable long-term operation.

Based on existing knowledge of PA 3200 GF and tests of additively manufactured bearings, this paper examines SLS-manufactured PA 3200 GF sliding bearings under realistic operating conditions. The aim of this study is to quantify the evolution of the friction coefficient and contact temperature in several different PV regimes and to characterize changes in surface morphology based on pre- and post-test data. Moreover, the specific wear rate is determined and the main wear mechanisms are identified based on experimental examination of the worn bearing surfaces. Evaluation of long-term durability is not the focus of this study and will be explored in future research. Based on these findings, this study presents experimentally supported knowledge of how different loading regimes affect the tribological properties of SLS-fabricated sliding bearings under dry-sliding conditions, thus providing a clearer understanding relevant to environmentally oriented machine design.

2. Materials and Methods

In this section, a detailed overview of the material used, the manufacturing procedure, the experimental setup, the measurement techniques, and the test conditions will be specified. The aim of this chapter is to define how the PA 3200 GF bearings were made, the way in which the tribological measurements were performed, and the PV regimes under which the tests were performed, ensuring full transparency and reproducibility of the experiment methodology.

2.1. Material Description

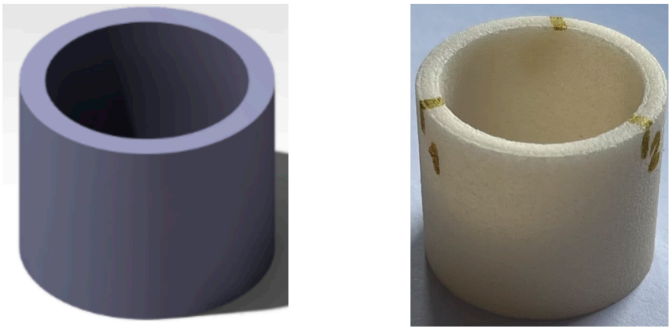
The sample bearings were produced from PA 3200 GF (EOS GmbH, Krailling, Germany), a polyamide 12 matrix reinforced with 40 wt% glass beads. This composite material is characterized by increased stiffness while maintaining sufficient elasticity to ensure stable performance at elevated temperatures. Due to its improved mechanical properties and wear resistance, PA 3200 GF is successfully applied for machine parts under higher loads, making

it a suitable choice for the plain bearings tested in this work. The material properties [25] are summarized in Table 1.

Table 1. Mechanical and thermal properties of PA 3200 GF.

Material Properties	Value	Standard
Tensile Modulus (z orientation) [Mpa]	2500	EN ISO 527-1/-2 [26]
Tensile Strength (z orientation) [Mpa]	47	EN ISO 527-1/-2 [26]
Hardness (Shore D)	80	EN ISO 48-4:2018 [27]
Temperature of Deflection under Load 1.80 Mpa [°C]	96	EN ISO 75-1/-2 [28]
Temperature of Deflection under Load 0.45 Mpa [°C]	157	EN ISO 75-1/-2 [28]
Powder color	whitish	/
Density [g/cm^3]	1.22	/

The investigated bearings have a nominal inner diameter of 20 mm, an outer diameter of 30 mm, and a length of 20 mm. These dimensions enable easy assembly while guaranteeing constant fit and uniform distribution of load throughout operation. All samples were printed along the *Z*-axis, selected due to the known influence of the print orientation on the mechanical and tribological properties of SLS-manufactured components. Measurements taken at three axial locations yielded an average inner diameter of $d = 20.18 \pm 0.034$ mm, which indicates adequate process repeatability and narrow tolerance distribution. Figure 1 shows the CAD model from which the STL file was used for the sample's SLS production.



(**a**) (**b**)

Figure 1. (**a**) CAD model of the bearing; (**b**) SLS-manufactured testing bearing.

The tested bearings are mounted on a sleeve made of stainless steel, with a mean diameter of 19.877 mm and a length of 37.25 mm, which achieved a loose fit with a mean value of clearance of 0.304 mm. The stainless-steel sleeve was polished to a smooth finish suitable for sliding bearing application and testing. The goal of the chosen geometry is to simulate realistic operating conditions.

2.2. Selective Laser Sintering of Sliding Bearings

The SLS technology, shown in Figure 2, was used for the production of parts, as it is one of the most reliable additive technologies for producing components with complex geometries. The powder sintering process uses a laser as an energy source to selectively melt material in accordance with a digital 3D model in STL format. After the completion of the melting of an individual layer, the building chamber is lowered by a predefined value, which enables the formation of the next layer. This process is repeated until the part is completely fabricated. SLS technology supports a broad range of polymer materials, including PA12, polyamide 11 (PA11), polypropylene (PP), thermoplastic polyurethane (TPU), and polyether ether ketone (PEEK), among others. The key advantages compared to other additive techniques are the possibilities of making parts of complex geometries

without the need for additional support structures and the reusage of powder, which reduces material consumption and shortens post-processing time [29].

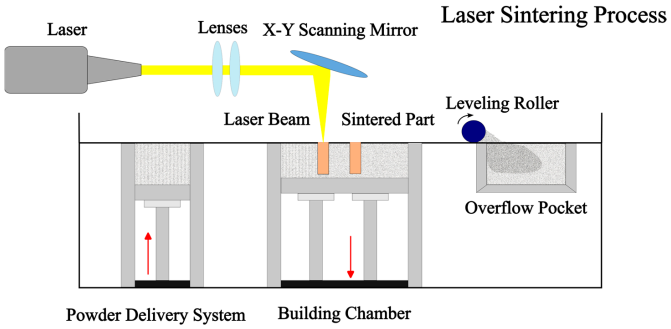


Figure 2. Selective Laser Sintering Process.

We fabricated the samples using the Formiga P100 SLS system (EOS GmbH). Manufacturer-recommended process settings were applied during the fabrication process, ensuring the highest quality and reliability of the resulting parts. All samples were fabricated in a single batch, ensuring uniform sintering conditions and thus uniformity of the properties of all tested bearings. The powder used as the material was 70% new and 30% used powder, in accordance with EOS recommendations for achieving optimal mechanical and tribological performance. The process parameters for SLS fabrication are shown in Table 2.

Table 2. Formiga P100 properties.

Effective building volume [mm]	200 × 250 × 330
Layer thickness [mm]	0.1
Laser type [W]	30, CO_2
Precision optics	F-theta lens 80
Wavelength of laser [µm]	10.6

2.3. Experimental Setup

The tribological characteristics of sliding bearings were investigated on the USL 5-30 device, Figure 3, developed at the Faculty of Mechanical Engineering, University of Belgrade. The tested bearing was installed in a subassembly consisting of a sleeve, a rolling bearing, and a driven console. The rotation is provided by an electric motor connected by a belt transmission to the sleeve on which the sleeves are located. The friction-generated torque was transferred to a driven console resting on a measuring console with built-in strain gauges, arranged in Wheatstone's bridge, which allows registration of the friction torque. The angular speed of the sleeve is regulated by a frequency regulator (AEG Microverter D 2.8/230 V), while the radial load is introduced by a lever system. Weights are placed on the free end of the lever, which generates a radial force on the subassembly with a sliding bearing in a lever ratio of 1:10.

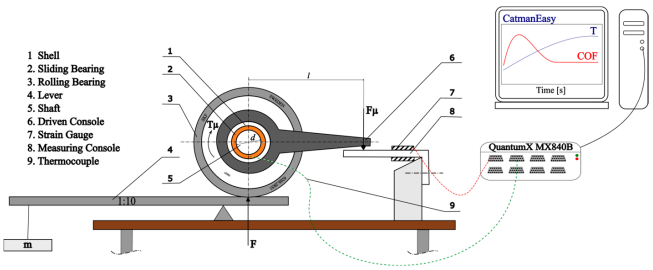


Figure 3. USL 5-30 testing setup.

Unlike conventional tribological tests, such as pin-on-disc or block-on-disc tests, this procedure analyzes real machine parts instead of pin or disc specimens. Consequently, the actual contact between the inner and outer cylinders is taken into account, as well as the characteristic pressure distribution on the side where the radial force acts.

2.4. Experimental Measurements

The tests were performed to determine the coefficient of friction, contact temperature, wear rate, and surface evolution of the sliding bearing during interaction with a sleeve made of stainless steel.

The coefficient of friction was determined indirectly, through the frictional moment transformed from the moving console to the measuring console. Four strain gauges, CLY41–6/120ZE (HBM), each with a nominal resistance of 120 Ω, connected in a full Wheatstone bridge, are placed on the measuring console. This configuration enables maximum sensitivity in the measuring system and simultaneous temperature compensation, because all four branches actively participate in the registration of the resistance change caused by the friction moment.

Contact temperature was measured using a K-type thermocouple, TF-50 (PeakTech Prüf- und Messtechnik GmbH, Ahrensburg, Germany), embedded in the sliding bearing. The sensor allows a measurement range from −40 to 204 °C, with an accuracy of ±0.5% of the reading value. A blind hole with a diameter and depth of the tip of the thermocouple is positioned at a distance of 1–1.5 mm from the sleeve-bearing contact surface. The hole, where the embedded tip is located, is at the mid-width of the front outer bearing surface. This configuration enables stable mechanical fixation and excellent temperature contact between the sensor and the tested bearing. The measured temperature represents the bearing temperature close to the sleeve-bearing sliding interface, which reliably reflects the thermomechanical response of the bearing in dry sliding conditions.

The mass of the samples was determined on a Mettler B6 mechanical analytical balance (Mettler-Toledo International Inc., Greifensee, Switzerland), with a resolution of 0.1 mg and a maximum capacity of 100 g. The average measured mass of the PA 3200 GF sliding bearing was $m = 4.1404 \pm 0.1303$ g. The analytical balance's high resolution allowed for the precise measurement of mass loss of the samples after tribological testing.

Surface roughness was measured using a MarSurf SD26 (Mahr GmbH, Göttingen, Germany) contact profilometer at three characteristic measuring points on the inner bearing surface, evenly distributed at an angle of 120°. The traversing length was 5.6 mm, with a sampling length of 2.5 mm and a cutoff of 0.8 mm, resulting in a total of 11199 measuring points per measuring line according to the ISO 21920-3 standard [30]. The parameters R_a, R_k, R_{pk}, and R_{vk}were determined on each measuring trace based on the ISO 21920-2 [31] standard, which allows a detailed assessment of the condition of the bearing surface before and after testing.

The QuantumX MX840B (Hottinger Baldwin Messtechnik, Darmstadt, Germany) module was used for data acquisition, enabling simultaneous recording of signals from eight different sensors. In this study, strain gauge and thermocouple signals were acquired in parallel. Data acquisition was carried out with a sampling frequency of 1 Hz, while the signal was processed through a built-in active low-pass filter automatically adapted to the sampling frequency. The obtained signals are monitored and stored in real time using the software package catmanEasy/AP (version 4.1.1.17, Hottinger Baldwin Messtechnik GmbH, Darmstadt, Germany), which provides visualization, calibration of the measuring channels, and data export for further analysis. This system enabled reliable detection of both short-term oscillations and long-term trends during the entire duration of the tribological tests.

Before SEM imaging using Tescan MIRA3 (TESCAN Group a.s., Brno, Czech Republic), the selected representative samples were sputter-coated with a thin gold layer using a Polaron SC503 (Fisons Instruments, Ipswich, UK) sputter coater to minimize electrostatic charging during SEM analysis. SEM analysis offers a more detailed look at the surface morphology, wear mechanism and manufacturing quality of the SLS-fabricated bearings.

2.5. Experimental Conditions

The experimentally obtained results provide insight into the tribological characteristics of the SLS-fabricated composite PA 3200 GF bearing. The tests were carried out under dry-sliding conditions, in contact with a stainless-steel sleeve.

Three pressure (P) and velocity (V) regimes, given in Table 3, were applied to enable an analysis of bearing behavior under varying PV conditions. The selected regimes are defined based on literature precedent for SLS composites made with PA12 base tested in dry-sliding condition. Previous studies show a PV value of 1 MPa·ms^{-1} as heavily loaded operating conditions [14,16]. Accordingly, this regime is defined as a high PV regime, while the other regimes are chosen proportionally and relatively in relation to this one and classified as medium and low PV. For each PV regime, three independent tests were conducted using new samples. To minimize potential bias associated with the order of performance, the order of tests was randomized. The complete PV characteristic of the bearing was beyond the scope of this research and remains the focus of future investigations.

Table 3. Experimental conditions of PA 3200 GF sliding bearings.

Material Properties	Regime I	Regime II	Regime III
Radial Load [N]	400	300	200
Pressure [MPa]	1	0.75	0.5
Peripheral speed [m·s^{-1}]	1	0.75	0.5
Sliding Distance [m]	3600	2700	1800
Test Duration [s]	3600	3600	3600
Ambient temperature [°C]	23–26	23–26	23–26

All tests were performed under laboratory conditions at a typical indoor relative humidity of 30%. Before and after testing, all samples were cleaned in an ultrasonic bath (ASonic Ultrasonic Cleaner PRO90) using petroleum ether as a medium for 30 min at a temperature of 45 °C to remove residual dust and potential contaminants. After cleaning, the samples were air-dried at a temperature of 25 °C and 30% relative humidity. To remove moisture from the surface pores, it was dried in a dryer for 2 h at a temperature of 40 °C without affecting mechanical properties.

3. Results and Discussion

The results presented in this section show the tribological response of SLS-manufactured PA 3200 GF sliding bearings, with a focus on the effect of different PV regimes on COF, temperature, wear behavior, and surface change in dry-sliding conditions.

3.1. Time Evolution of COF and Temperature

The aim of this section is to present time-dependent coefficients of friction and temperature for examined PV regimes in order to understand their mutual dependence. After acquisition, the data were analyzed using the MATLAB (version 2024b, The MathWorks, Inc., Natick, MA, USA) software package.

Before processing, the signals obtained from the sensors were filtered using an active low-pass filter to remove noise and ensure the actual measured values. Figures 4–6 show

the experimentally measured trends of the coefficient of friction and temperature as a function of time. The total duration of each test was 3600 s, which was enough to reach the steady-state of the system. Tests for all regimes were performed in triplicate. All graphs clearly show the characteristic two phases of tribological behavior:

- the running-in phase, during which adaptation and alignment of the surfaces in contact occur,
- steady-state phase, in which the contact reaches mechanical and thermal equilibrium.
- At the beginning of sliding, the bearing surface of the polymer bearing is relatively rough with pronounced asperities, which leads to discontinuity in the contact between the bearing and the sleeve. In this phase, there is an increased share of mechanical interlocking, when material irregularities remain trapped within each other, resulting in increased friction and pronounced oscillations. Therefore, the actual contact surface is initially significantly smaller than the nominally calculated one, because the contact is made on the tops of the asperities. As the test continues, under the influence of radial load and speed designated as the PV regime, the asperities are mechanically cut off, deformed, and worn, which increases the effective area in contact. This process of smoothing the surface leads to a gradual decrease and stabilization of the friction coefficient, which is clearly observed in the COF and T trend diagrams.

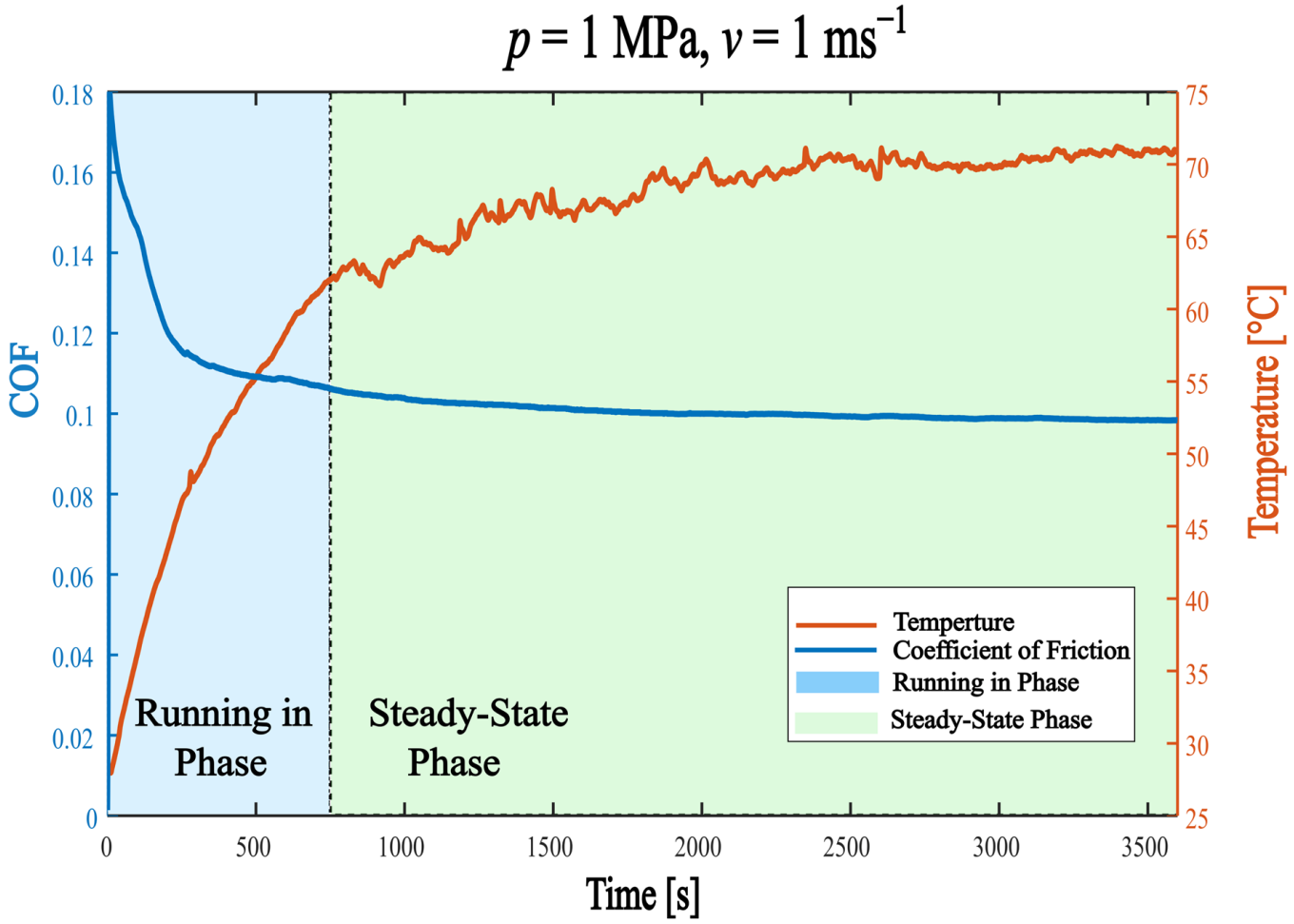


Figure 4. COF and Temperature trend for Regime I (representative curve from one of the three repeated tests).

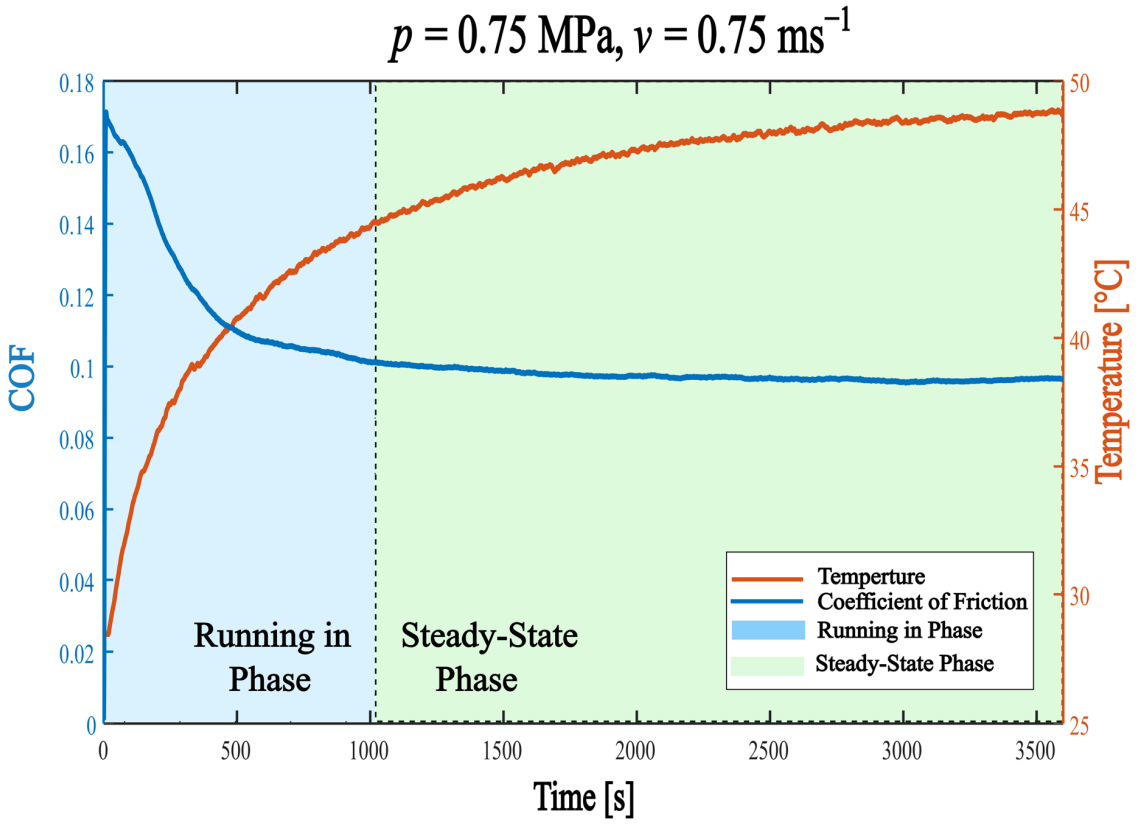


Figure 5. COF and Temperature trend for Regime II (representative curve from one of the three repeated tests).

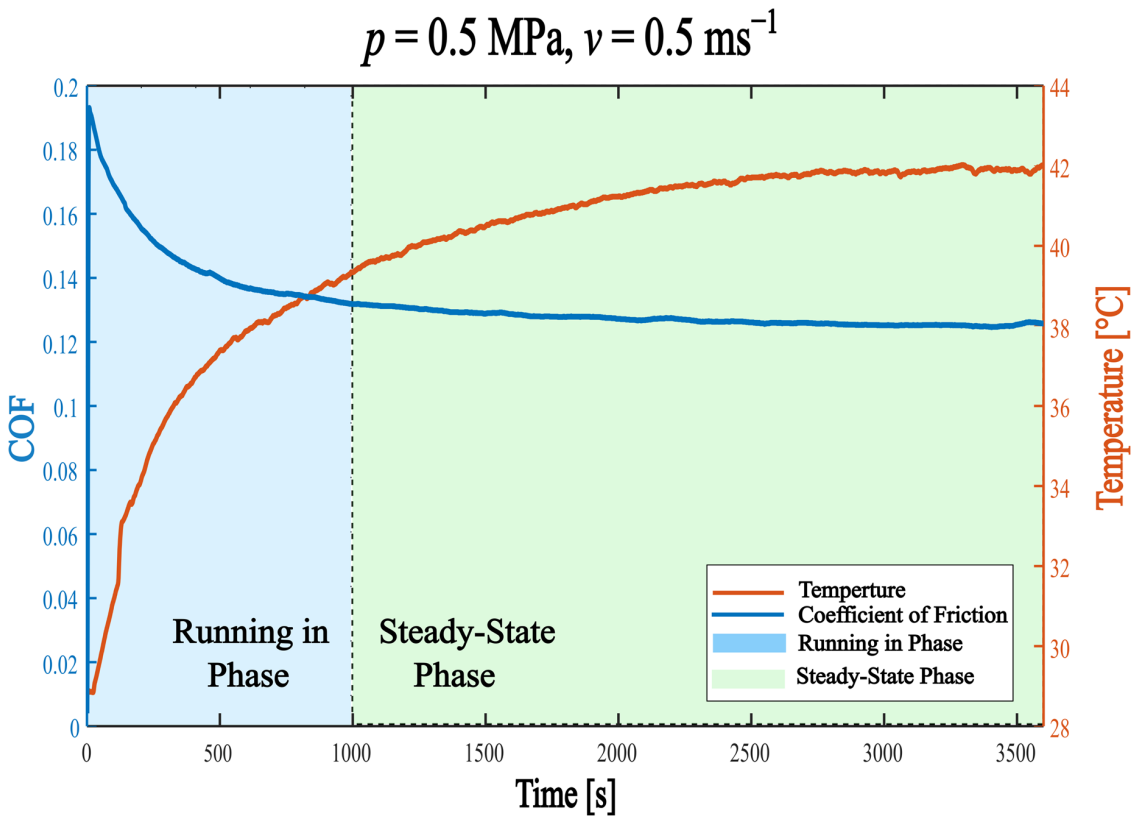


Figure 6. COF and Temperature trend for Regime III (representative curve from one of the three repeated tests).

Figure 4 shows a representative graph of COF and T evolution for Regime I (p = 1 MPa, v = 1 m·s^{-1}) which represents the most heavily loaded regime. In the initial phase of the test, there is a sudden increase in COF to a maximum value of 0.1798, after which the coefficient of friction starts to decrease. This sudden increase and drop in the coefficient of friction indicates the running-in phase. In Regime I, the running-in phase takes ≈960 s, after which the COF settles at ≈0.09. The temperature has an amplitude of change of 43.23 °C, from an initial temperature of 27.99 °C to a maximum temperature of 71.22 °C.

The evolution of friction and temperature for moderately loaded Regime II (p = 0.75 MPa, v = 0.75 m·s^{-1}) is shown in Figure 5. During the running-in period, which lasts ≈ 1080 s, the COF reaches a maximum value of 0.1712 before gradually decreasing to a stable value of ≈0.09. This reduction in COF indicates progressive surface polishing and real contact stabilization between the bearing and sleeve. During the test, the contact temperature increases from 28.46 °C to 48.86 °C, which represents a moderate increase corresponding to the medium PV regime. Stable COF and moderate temperature oscillations confirm balanced heat generation and dissipation during steady operation.

Figure 6 shows the time-dependent change in COF and T for the least loaded Regime III (p = 0.5 MPa, v = 0.5 m·s^{-1}). The COF initially increases to a value of 0.1931 and subsequently decreases to a steady-state level of approximately 0.12 after a running-in period of ≈1000 s. The observed behavior shows slower surface adaptation due to lower contact pressure and speed. During this interval, the temperature rises moderately from 28.85 °C to 42.02 °C, maintaining good thermal stability and confirming the mild friction conditions typical for low PV regimes.

Throughout the duration of the test, COF and T show mutual dependence. The drop in COF during the running-in period coincides with a sharp increase in temperature, after which both parameters reach stable values. This phenomenon indicates the formation of a stable zone of contact between the bearing and sleeve, in which the processes of heat generation and dissipation are balanced. In all tested regimes, the COF stabilization moment corresponds to the temperature stabilization, which confirms that the friction and the temperature of the PA 3200 GF bearing are interrelated.

A comparative analysis of the three PV regimes indicates a clear pattern of tribological behavior. Higher PV values lead to a shorter running-in period, a lower stable COF, and a higher contact temperature as a consequence of increased heat generation by limited dissipation. Conversely, lower PV values result in a longer period of adaptation of the contact surfaces, as well as a higher stable COF, but with less temperature rise and thermally more stable behavior in the steady-state. The intermediate regime shows the most favorable relationship between the coefficient of friction and thermal stability, which can be considered the favorable operating condition for PA 3200 GF bearings in dry-sliding conditions.

3.2. Steady-State Comparison

Steady-state values of friction coefficient and contact temperature were determined in triplicate for all regimes, given in Figure 7. The steady-state interval was defined in the last quarter of each test (900 data points), in which the system reached thermal and mechanical equilibrium, to avoid the effects of the transition phase. Mean values of COF and T were calculated for each test separately.

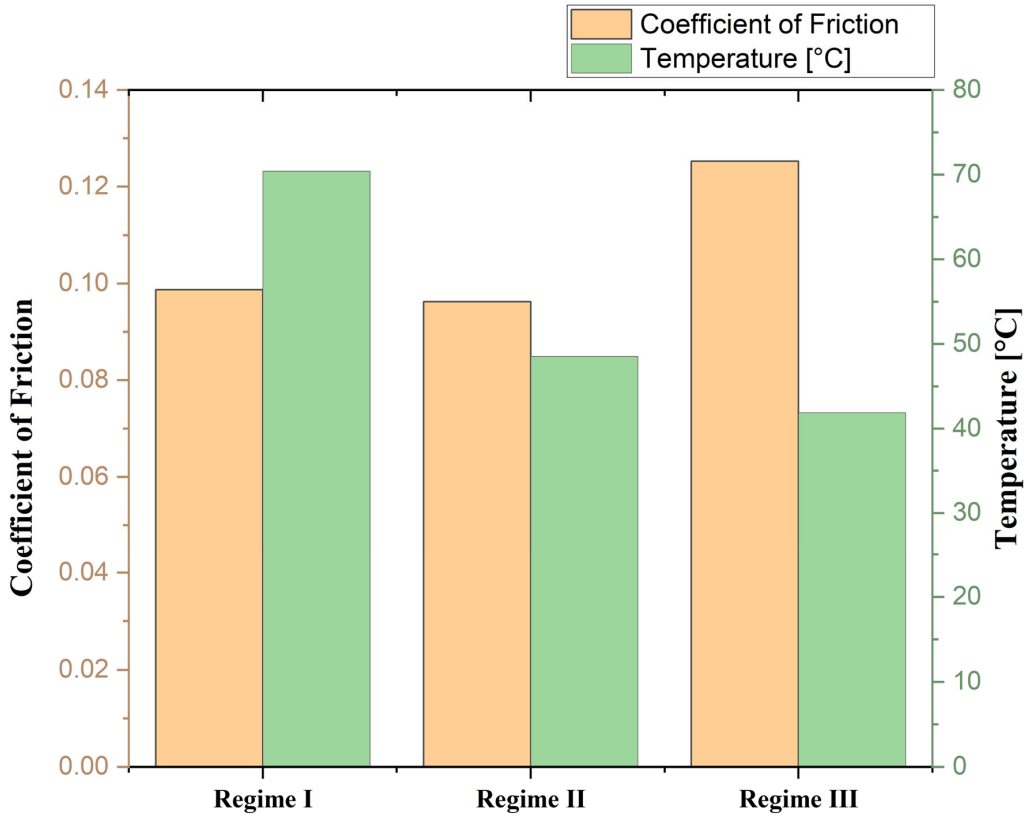


Figure 7. Steady-state mean COF and T for all regimes.

Table 4 summarizes the results of the tribological test. Among the tested conditions, Regime II shows the best balance between friction and thermal stability, with the lowest mean COF and mean temperature increase. Regime I, with the highest level of PV, shows a comparative COF but with a significantly higher mean temperature increase, which may be a consequence of limited heat dissipation. Regime III, at the lowest PV values, shows a slightly higher COF followed by the lowest contact temperature, which indicates a reduction in frictional energy generation but with insufficient load that leads to incomplete surface conformity. In all PV regimes, the measured temperatures during operation remain below the critical thermal limits determined for PA 3200 GF material, i.e., below ≈96 °C and ≈157 °C [25], at which softening, stiffness decrease, and unwanted changes in bearing geometry may occur. As sliding continues, local temperature rise becomes an important factor that can significantly affect system performance. Polymers are generally more thermomechanically sensitive than metals, and elevated temperatures can lead to softening if the Vicat softening temperature is exceeded, which can result in an increase in the actual contact area and even local melting and adhesive wear. Studies of polymer materials [32] show that if the temperature limits are moderate, this process can contribute to stabilization friction through the creation of a homogeneous transfer film.

Table 4. Experimental results for all regimes.

Regime	P [MPa]	V [m·s^{-1}]	μ_{max}	μ_{ss}	$\sigma(\mu)$	T_{max} [°C]	T_{ss} [°C]	$\sigma(T)$ [°C]	t_{RI} [s]
I	1	1	0.1798	0.0987	0.0002	71.22	70.41	0.45	960
II	0.75	0.75	0.1712	0.0962	0.0003	48.86	48.52	0.18	1080
III	0.5	0.5	0.1931	0.1253	0.0003	42.02	41.88	0.05	1000

The standard deviations of the COF, and temperature within the steady-state interval were less than 0.0003 and less than 0.5 °C, respectively, indicating minimal oscillations and

stable contact conditions. These values represent the within-run standard deviation and confirm that the PA 3200 GF plain bearings achieve a very consistent tribological response after establishing a stable operating regime. Variations in mean steady-state values of COF and T for three repetitions per regime are small compared to differences between regimes, which indicates satisfactory reproducibility of tribological performance.

Overall, the comparison of steady-state values confirms that the tribological behavior of the PA 3200 GF bearing is stable and predictable under dry-sliding conditions. Considering only friction and temperature, Regime II was the most favorable. However, according to the results of the surface morphology analysis shown in Section 3.3, this regime results in the largest increase in the peak and core parameters. Therefore, the suitable PV regime depends on the balance of low friction, temperature stability, and surface integrity required for a particular application. Comparing the results with PA12 [24], PA 3200 GF bearings shows a negligibly higher COF in the most loaded regime but with significantly better thermal stability during all regimes and a more favorable COF-T balance.

3.3. Wear Behavior and Wear Mechanism of PA 3200 GF Sliding Bearings

Wear behavior of SLS-manufactured PA 3200 GF sliding bearings is quantified by determining the specific wear rate by measuring the mass loss after tribological testing. This approach was chosen as an already widely accepted standard in polymer tribology, where the absolute change in volume is often tiny and difficult to measure with adequate accuracy due to the pronounced elasticity of the material, surface irregularity, and the formation of wear products. Therefore, the method based on mass loss represents a reliable and reproducible way for comparative wear analysis under controlled conditions.

Specific wear rate W_s is determined as [33]:

$$W_s = \frac{\Delta m}{\rho \cdot F \cdot L} \tag{1}$$

where Δm [g] is the mass loss, ρ $\left[\mathrm{g/mm^3}\right]$ is the material density, F [N] is the applied radial force, and L [m] is the total sliding length. The specific wear rate was determined based on the mass loss after 2 hours of the experiment. The extended duration of the test was applied to increase the measurement reliability of the wear rate, since there will be a cumulative increase in mass loss, and the coefficient of friction and the temperature remain unchanged compared to the stationary state achieved in the first hour.

The specific wear rate results for different PV regimes are given in Figure 8.

The results show that the medium Regime II has the lowest specific wear rate, which shows that it best balances the applied load and speed. Conversely, the least loaded regime has the highest specific wear rate, despite the reduced load, indicating that wear is not only influenced by pressure and speed. Relatively large scatter in Regime III shows that there is reduced wear stability, likely caused by intermittent micro-contact, heterogeneous pressure distribution between polymer and glass balls, local stress concentrations, and the sintering process itself, which is heterogeneous on the surface, and therefore balls that are not completely solidified by polymer may fall off. The highest PV regime shows the most repeatable behavior due to wear, which is characterized by a smaller scatter, which may be a consequence of achieving a better and more stable contact. The results show that for SLS-manufactured PA 3200 GF sliding bearings operating in dry sliding conditions, wear behavior is a consequence of contact stability and tribological adaptation of the bearing surface, rather than the load itself. The wear trend is consistent with the friction coefficient trend, and low values indicate stable sliding and controlled material removal. The presented results are limited to the number of samples, investigated PV regimes, and

dry sliding conditions. Extrapolation of these tests to other working conditions should be done with extreme caution and be supported by additional experimental tests.

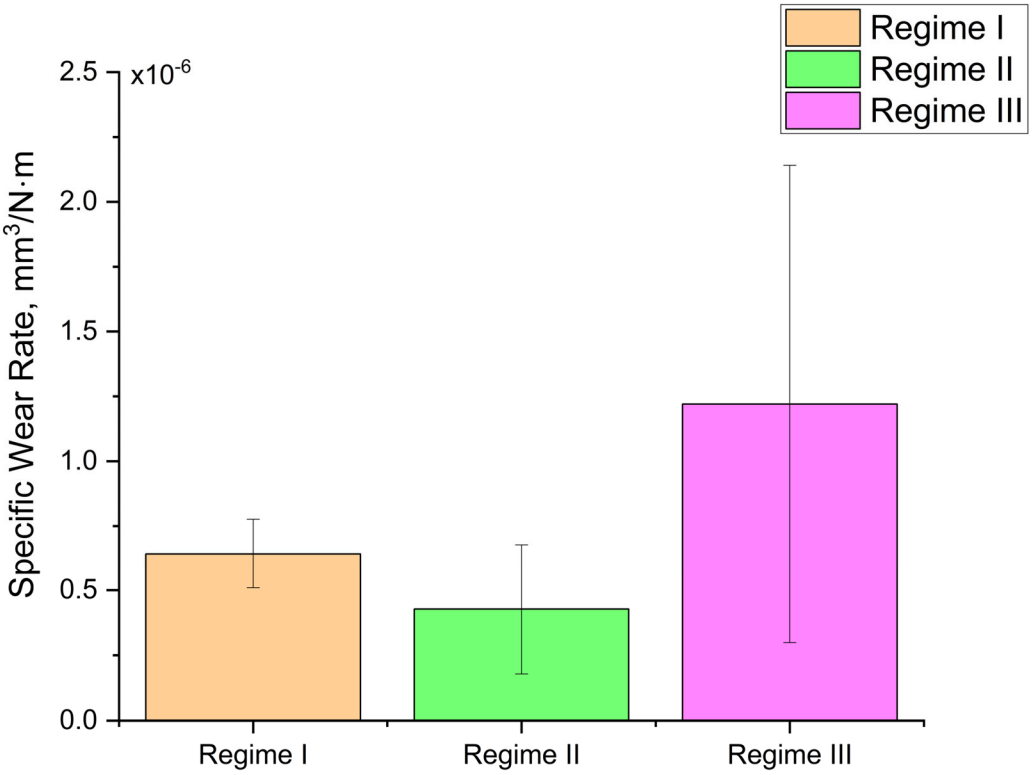
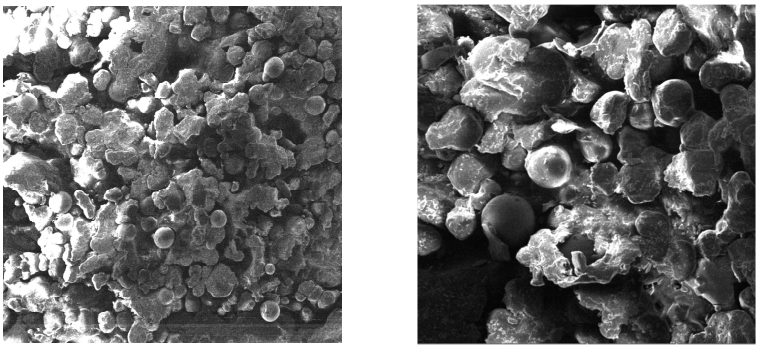


Figure 8. Specific wear rate of PA 3200 GF sliding bearing.

Figure 9 shows SEM images exhibiting the characteristic microstructure of the SLS-manufactured PA 3200 GF sliding bearing after sintering. SEM was used to determine the quality of sintering and to see the surface morphology of the bearing. Both enlargements show that the surface is formed by agglomerates of partially coalesced powder particles, connected by sintered necks, with a pronounced presence of interparticle pores and cavities. At higher magnification (500×), flattened zones of melted powder can be observed, in which almost intact spherical particles of the glass ball are trapped. Such a porous and granular surface morphology directly explains the high initial values of roughness parameters.



(**a**) (**b**)

Figure 9. SEM images of bearing surface (**a**) 200× magnification; (**b**) 500× magnification.

A wear mechanism on the bearing surface was analyzed using SEM. Figure 10 clearly shows the change in surface morphology as a consequence of predominantly adhesive wear with plastic deformation and cladding of asperities. Plastic deformation occurred as a result of shear stresses due to sliding, which leads to detachment of wear debris. By

increasing the load, adhesion junctions expand, and the dominant wear mechanism does not change, but only morphological intensification does. Therefore, differences between PV regimes are reflected primarily in the intensity and morphology of wear features rather than in a transition of the dominant wear mechanism. Some scratch marks were observed, which may be due to glass debris, which may act as abrasive particles. On the surface of the glass balls, you can see a clear alignment as a result of the wear of the glass balls, which are worn abrasively, which can also be seen by the presence of parallel furrows. Features consistent with accumulated wear debris and smeared polymer layers were observed on the surface.

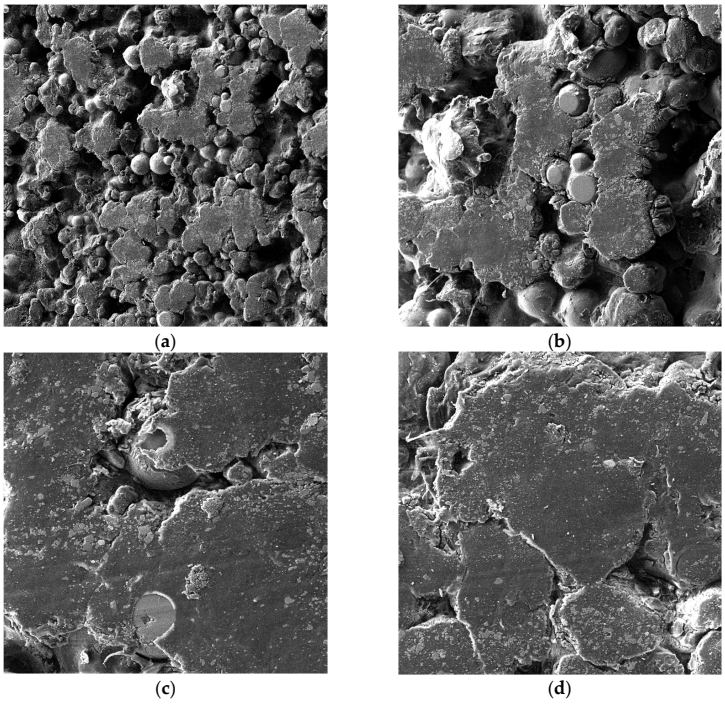


Figure 10. SEM images of tribo-surface of sliding bearing (**a**) 200× magnification; (**b**) 512× magnification; (**c**) 990× magnification; (**d**) 1000× magnification.

3.4. Surface Roughness Evolution of PA 3200 GF Bearings

Surface topography is one of the critical factors in the tribology of 3D-printed sliding bearings under dry-sliding conditions, as it has a direct impact on friction, wear, heat generation, and generally on the service life of the bearing. Adjusting these parameters through the printing process itself and post-processing can improve tribological performance.

In dry-sliding conditions, the surface topography goes through a period of adaptation due to removal of peaks, plastic deformation, and filling of micro-bays on the surface. R_a was used as the basic descriptive parameter of the roughness level, while Abbott-Firestone family (R_k) parameters (R_k, R_{pk}, R_{vk}) were analyzed as functional parameters relevant for tribological behavior. R_{pk} describes the peaks of the profile that can be removed during the running-in period and contact stabilization, R_k represents the load-carrying core of the profile that supports the mechanical load during operation, while R_{vk} indicates the capacity of the surface to retain worn material. The analysis of these parameters enables the engineering interpretation of running-in, load distribution, and long-term surface resistance during exploitation.

Table 5 shows the average values of roughness parameters. The initial topography of SLS-manufactured bearings is characterized by a rough surface with pronounced cores and moderate peaks. The high load-carrying part of the surface with the presence of valleys

indicates that after removing the peak asperities during the running-in phase, the surface can provide stable contact and favorable load-carrying in dry-sliding conditions.

Table 5. Average surface roughness parameters before and after testing with standard deviation.

Condition	R_a	R_k	R_{pk}	R_{vk}
Before testing	12.343 ± 2.23	39.48 ± 8.89	11.24 ± 3.91	22.20 ± 7.16
After testing	12.12 ± 2.09	36.95 ± 8.69	10.37 ± 4.32	22.85 ± 6.02

Percentage change in roughness parameters by regime in Figure 11 offers a more comprehensive understanding of the profile change.

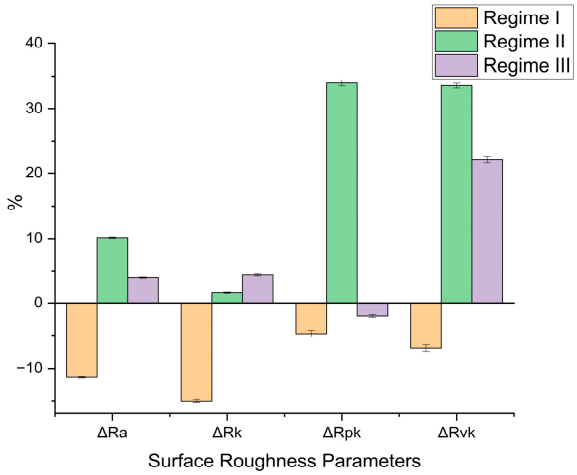


Figure 11. Percentage change in surface roughness parameters after testing.

In Regime I, the average negative changes of R_a and R_k indicate a general smoothing of the surface and a reduction in the core roughness depth, which shows that the load-carrying backbone of the surface becomes more uniform after operation. A moderate pair of R_{pk} and R_{vk} indicates that the peaks of asperities that affect initial wear and the valleys into which wear debris enters are reduced. Taking everything into account, the reduction in all parameters indicates a flatter surface with a narrower roughness amplitude range, which enables a more even load distribution and a reduced risk of local failure.

In Regime II, R_a and R_k increase, which indicates a rougher surface with enhanced core roughness compared to the initial state. The reported rise in R_{pk} and R_{vk} indicates that both asperity peaks and valleys become more pronounced in relation to the core, indicating greater peak prominence and deeper valleys. The average increase of R_a, R_k, R_{pk} and R_{vk} indicates a surface topography with a more intensified height contrast, where roughness amplitudes dominate in relation to surface smoothness.

Regime III is characterized by a marginal increase in R_a and R_k which indicates that the surface remains relatively rough after work, followed by a small expansion in the core roughness depth. Increased R_{pk} values indicate that the peaks have partially degraded, followed by an increase in R_{vk} values, which indicates the formation of deeper valleys. Overall, the combined behavior of the parameters shows an asymmetric surface topography where valleys dominate over peaks, characteristic of lower loads where peak removal occurs without substantial core flattening.

The most favorable behavior is in Regime I, where most of the surface parameters decrease and the supporting surface stabilizes. Regime III, as the least loaded, provides moderate changes without significantly disturbing the profile. The most unfavorable

regime from the aspect of the surface roughness is Regime II, where there was the most pronounced deviation of the surface in relation to the initial state.

The coefficient of friction and the temperature increase correlate with the mechanism of change in the surface morphology of the PA 3200 GF bearing during operation. In the most loaded regime, the rapid formation of the steady-state COF corresponds to decreases in R_a and R_k which means the effective smoothing of the asperities and the consolidation of the bearing core. At the same time, R_{pk} and controlled R_{vk} allow for stable debris accommodation and clarify the elevated but consistent temperature plateau. In the lowest regime, the moderate temperature increase and slower running-in coincide with the moderate changes in roughness, where the peaks are slightly flattened and the valleys are deepened, which leads to a moderately higher COF due to slightly less real contact. The medium PV regime is characterized by the largest increase in R_k, R_{pk}, and R_{vk} despite the low COF. The results indicate that favorable friction alone is not enough; the most suitable bearing performance requires a balanced coevolution of the coefficient of friction, temperature, and roughness parameters within a stable thermomechanical regime.

4. Conclusions

The study of SLS-manufactured bearings made of PA 3200 GF shows that the results obtained demonstrate reliable operation within the framework of the tested PV regimes. In all tested PV regimes, a clear transition from the running-in phase to stable operating conditions was observed, followed by low fluctuations of the friction coefficient and contact temperature. An increase in the PV regime leads to a shortening of the running-in period and lower friction values in the steady state, but with increased contact temperatures. In contrast, lower PV regimes reduce the thermal load but result in more pronounced changes in the roughness parameters that describe the core of the profile and the tops of the asperities. The wear analysis showed that the stability of the contact and the adaptation of the surface have a greater influence on the mass loss than the magnitude of the load itself. The evolution of the surface roughness and SEM analysis indicate dominant adhesive wear with localized abrasive contributions of glass balls, while the change in the dominant wear mechanism with the change in PV regime was not observed. The obtained results confirm that the frictional characteristics alone are not sufficient to define the suitable operating conditions, but PV regimes must be considered integrated through friction, temperature, wear rate, and surface topography. The importance of this research is in the testing of real machine elements and the expansion of knowledge beyond conventional testing methods as well as tests closer to the real use of machine elements, in this case sliding bearings.

Author Contributions: Conceptualization, I.S., D.M., Ž.M. and A.M.; methodology, I.S., A.M., Ž.M. and D.M.; software, I.S., Ž.M. and D.M.; formal analysis, I.S.; investigation, I.S., Ž.M. and A.M.; resources, I.S., Ž.M. and D.M.; writing—original draft preparation, I.S.; writing—review and editing, I.S., A.M. and D.M.; visualization, I.S.; supervision, A.M. and D.M. All authors have read and agreed to the published version of the manuscript.

Funding: This research was funded by the Ministry of Science, Technological Development and Innovation of the Republic of Serbia under the Agreement on financing the scientific research work of teaching staff at accredited higher education institutions in 2025, No. 451-03-137/2025-03/200105, dated 4 February 2025.

Data Availability Statement: The original contributions presented in this study are included in the article. Further information is available from the corresponding author upon request.

Acknowledgments: The results presented in this paper are the results of research supported by the Ministry of Science, Technological Development and Innovation of the Republic of Serbia under the Agreement on financing the scientific research work of teaching staff at accredited higher education institutions (Contract No. 451-03-137/2025-03/200105 dated 4 February 2025) and CA23155—A pan-European network of Ocean Tribology (OTC). The authors express gratitude to the "3D IMPULSE" laboratory for supplying all specimens utilized in this research.

Conflicts of Interest: The authors declare no conflicts of interest.

References

1. Du, F.; Li, D.; Sa, X.; Li, C.; Yu, Y.; Li, C.; Wang, J.; Wang, W. Overview of Friction and Wear Performance of Sliding Bearings. *Coatings* **2022**, *12*, 1303. [CrossRef]
2. Marinković, A.; Stojanović, B.; Gachot, C.; Lazović, T. Analysis of Lubrication Regimes for Porous Sliding Bearing. *Lubricants* **2024**, *12*, 184. [CrossRef]
3. Friedrich, K. Polymer Composites for Tribological Applications. *Adv. Ind. Eng. Polym. Res.* **2018**, *1*, 3–39. [CrossRef]
4. Lawrowski, Z. Polymers in the Construction of Serviceless Sliding Bearings. *Arch. Civ. Mech. Eng.* **2007**, *7*, 139–150. [CrossRef]
5. Kim, S.S.; Shin, M.W.; Jang, H. Tribological Properties of Short Glass Fiber Reinforced Polyamide 12 Sliding on Medium Carbon Steel. *Wear* **2012**, *274–275*, 34–42. [CrossRef]
6. Bai, J.; Song, J.; Wei, J. Tribological and Mechanical Properties of MoS2 Enhanced Polyamide 12 for Selective Laser Sintering. *J. Mater. Process. Technol.* **2019**, *264*, 382–388. [CrossRef]
7. Gadelmoula, A.; Aldahash, S.A. Effect of Reinforcement with Short Carbon Fibers on the Friction and Wear Resistance of Additively Manufactured PA12. *Polymers* **2023**, *15*, 3187. [CrossRef]
8. Clavería, I.; Gimeno, S.; Miguel, I.; Mendoza, G.; Lostalé, A.; Fernández, Á.; Castell, P.; Elduque, D. Tribological Performance of Nylon Composites with Nanoadditives for Self-Lubrication Purposes. *Polymers* **2020**, *12*, 2253. [CrossRef]
9. Han, W.; Kong, L.; Xu, M. Advances in Selective Laser Sintering of Polymers. *Int. J. Extrem. Manuf.* **2022**, *4*, 042002. [CrossRef]
10. Rajendran, P.; Ganesan, A. Experimental Investigation on Friction Behavior of Selective Laser Sintering Processed Parts. *3D Print. Addit. Manuf.* **2024**, *11*, e1186–e1195. [CrossRef]
11. El Magri, A.; Bencaid, S.E.; Vanaei, H.R.; Vaudreuil, S. Effects of Laser Power and Hatch Orientation on Final Properties of PA12 Parts Produced by Selective Laser Sintering. *Polymers* **2022**, *14*, 3674. [CrossRef]
12. Liu, Y.; Zhu, L.; Zhou, L.; Li, Y. Microstructure and Mechanical Properties of Reinforced Polyamide 12 Composites Prepared by Laser Additive Manufacturing. *Rapid Prototyp. J.* **2019**, *25*, 1127–1134. [CrossRef]
13. Mousa, A.A.; Pham, D.T.; Shwe, S.P. Pre-Processing Studies for Selective Laser Sintering of Glass Beads-Filled Polyamide 12 Composites. *Int. J. Rapid Manuf.* **2014**, *4*, 28. [CrossRef]
14. Gadelmoula, A.; Aldahash, S.A. Tribological Properties of Glass Bead-Filled Polyamide 12 Composite Manufactured by Selective Laser Sintering. *Polymers* **2023**, *15*, 1268. [CrossRef] [PubMed]
15. Nar, K.; Majewski, C.; Lewis, R. Evaluating the Effect of Solid Lubricant Inclusion on the Friction and Wear Properties of Laser Sintered Polyamide-12 Components. *Wear* **2023**, *522*, 204873. [CrossRef]
16. Gadelmoula, A.; Aldahash, S.A. Dry Friction and Wear Behavior of Laser-Sintered Graphite/Carbon Fiber/Polyamide 12 Composite. *Polymers* **2023**, *15*, 3916. [CrossRef]
17. Bai, J.; Yuan, S.; Chow, W.; Chua, C.K.; Zhou, K.; Wei, J. Effect of Surface Orientation on the Tribological Properties of Laser Sintered Polyamide 12. *Polym. Test.* **2015**, *48*, 111–114. [CrossRef]
18. Cano, A.J.; Salazar, A.; Rodríguez, J. Effect of Temperature on the Fracture Behavior of Polyamide 12 and Glass-Filled Polyamide 12 Processed by Selective Laser Sintering. *Eng. Fract. Mech.* **2018**, *203*, 66–80. [CrossRef]
19. Vindokurov, I.; Khasyanov, R.; Pankov, A.; Strungar, E.; Tashkinov, M. Polyamide Composites Manufactured by Selective Laser Sintering: Effect of Glass Particle Reinforcement on Mechanical Properties. *Int. J. Adv. Manuf. Technol.* **2025**, *138*, 1413–1431. [CrossRef]
20. De Coninck, H.; Meyers, S.; Van Puyvelde, P.; Van Hooreweder, B. On the Difference in Mechanical Behavior of Glass Bead-Filled Polyamide 12 Specimens Produced by Laser Sintering and Injection Molding. *3D Print. Addit. Manuf.* **2024**, *11*, 419–433. [CrossRef]
21. Mourya, V.; Bhore, S.P.; Wandale, P.G. Comparative Investigation on Wear Properties of 3D-Printed Textured Journal Bearings. *J. Manuf. Process.* **2023**, *103*, 337–353. [CrossRef]
22. Lee, Y.-J.; Lee, K.-H.; Lee, C.-H. Self-Lubricating and Friction Performance of a Three-Dimensional-Printed Journal Bearing. *J. Tribol.* **2018**, *140*, 054501. [CrossRef]
23. Andrearczyk, A.; Bagiński, P. The Use of Additive Manufacturing Technology to Manufacture Slide Bearing Sleeves—A Preliminary Study. *Tribologia* **2020**, *291*, 7–14. [CrossRef]

24. Simonovic, I.; Marinkovic, A.; Milkovic, D.; Miskovic, Z.; Trajkovic, I.; Milosevic, M.; Milivojevic, A. Tribological Performance of Selective Laser Sintered Pa12 Sliding Bearings under Dry Sliding Conditions. *Sci. Sinter.* **2025**, 40. [CrossRef]
25. Rigid Glass-Filled Polyamide for 3D Printing. Available online: https://www.eos.info/polymer-solutions/polymer-materials/data-sheets/mds-pa-3200-gf (accessed on 20 November 2025).
26. *ISO 527-1:2019*; Plastics—Determination of Tensile Properties. Part 1: General Principles, 3rd ed. ISO: Geneva, Switzerland, 2019.
27. *ISO 48-4:2018*; Rubber, Vulcanized or Thermoplastic—Determination of Hardness—Part 4: Indentation Hardness by Durometer Method (Shore Hardness). ISO: Geneva, Switzerland, 2018.
28. *ISO 75-1:2020*; Plastics—Determination of Temperature of Deflection Under Load—Part 1: General Test Method. ISO: Geneva, Switzerland, 2020.
29. Yehia, H.M.; Hamada, A.; Sebaey, T.A.; Abd-Elaziem, W. Selective Laser Sintering of Polymers: Process Parameters, Machine Learning Approaches, and Future Directions. *J. Manuf. Mater. Process.* **2024**, *8*, 197. [CrossRef]
30. *ISO 21920-3:2021*; Geometrical Product Specifications (GPS)—Surface Texture: Profile—Part 3: Specification Operators. ISO: Geneva, Switzerland, 2021.
31. *ISO 21920-2:2022*; Geometrical Product Specifications (GPS)—Surface Texture: Profile—Part 2: Terms, Definitions and Surface Texture Parameters. ISO: Geneva, Switzerland, 2022.
32. Wu, W.; He, C.; Qiang, Y.; Peng, H.; Zhou, M. Polymer–Metal Interfacial Friction Characteristics under Ultrasonic Plasticizing Conditions: A United-Atom Molecular Dynamics Study. *Int. J. Mol. Sci.* **2022**, *23*, 2829. [CrossRef]
33. Sinha, S.K.; Briscoe, B.J. *Polymer Tribology*; Imperial College Press: London, UK, 2009; ISBN 978-1-84816-202-0.

Disclaimer/Publisher's Note: The statements, opinions and data contained in all publications are solely those of the individual author(s) and contributor(s) and not of MDPI and/or the editor(s). MDPI and/or the editor(s) disclaim responsibility for any injury to people or property resulting from any ideas, methods, instructions or products referred to in the content.